

Article

Determination of the Normalized Difference Vegetation Index (NDVI) with Top-of-Canopy (TOC) Reflectance from a KOMPSAT-3A Image Using Orfeo ToolBox (OTB) Extension

Kiwon Lee ^{1,*} , Kwangseob Kim ¹ , Sun-Gu Lee ² and Yongseung Kim ²

¹ Department of Electronics and Information Engineering, Hansung University, Seoul 02876, Korea; engintruder@hansung.ac.kr

² Korea Aerospace Research Institute, Satellite Application Division, Daejeon 34133, Korea; leesg@kari.re.kr (S.-G.L.); yskim@kari.re.kr (Y.K.)

* Correspondence: kilee@hansung.ac.kr; Tel.: +82-2-760-4254

Received: 19 March 2020; Accepted: 17 April 2020; Published: 18 April 2020



Abstract: Surface reflectance data obtained by the absolute atmospheric correction of satellite images are useful for land use applications. For Landsat and Sentinel-2 images, many radiometric processing methods exist, and the images are supported by most types of commercial and open-source software. However, multispectral KOMPSAT-3A images with a resolution of 2.2 m are currently lacking tools or open-source resources for obtaining top-of-canopy (TOC) reflectance data. In this study, an atmospheric correction module for KOMPSAT-3A images was newly implemented into the optical calibration algorithm in the Orfeo Toolbox (OTB), with a sensor model and spectral response data for KOMPSAT-3A. Using this module, named OTB extension for KOMPSAT-3A, experiments on the normalized difference vegetation index (NDVI) were conducted based on TOC reflectance data with or without aerosol properties from AERONET. The NDVI results for these atmospherically corrected data were compared with those from the dark object subtraction (DOS) scheme, a relative atmospheric correction method. The NDVI results obtained using TOC reflectance with or without the AERONET data were considerably different from the results obtained from the DOS scheme and the Landsat-8 surface reflectance of the Google Earth Engine (GEE). It was found that the utilization of the aerosol parameter of the AERONET data affects the NDVI results for KOMPSAT-3A images. The TOC reflectance of high-resolution satellite imagery ensures further precise analysis and the detailed interpretation of urban forestry or complex vegetation features.

Keywords: absolute atmospheric correction; KOMPSAT-3A; NDVI; Orfeo Toolbox; TOC reflectance

1. Introduction

There has been growing interest in the use of advanced information processing techniques such as big data and deep learning in working-level tasks dealing with satellite data, and the civilian and scientific applications of high-resolution satellite images extend to precise analyses of data to give insights beyond visual interpretation based on pixels. For optical images acquired from Earth observation (EO) satellites, precise analyses require processing to convert sensor radiance into scientific data such as atmospheric reflectance, surface reflectance, or surface temperature. Among the pre-processing procedures used for EO images, atmospheric correction is a core step in generating surface reflectance data. Satellite images for the application of these approaches should be provided with scientific data, such as surface reflectivity, rather than pixel-based image data.

Atmospherically corrected images are employed for many land use applications, such as quantitative vegetation metric estimation. The development of atmospheric correction schemes and their application models is still ongoing. Horion et al. [1] estimated normalized difference vegetation index (NDVI) values and analyzed the long-term trends in NDVI data derived from satellite sensors including SPOT-VEGETATION, Moderate Resolution Imaging Spectroradiometer (MODIS), and Advanced Very High Resolution Radiometer (AVHRR). Fan et al. [2] proposed temporally variable correction equations for generating long-term and consistent NDVI datasets from moderate-resolution sensors, such as AVHRR, MODIS, and Visible Infrared Imaging Radiometer Suite (VIIRS). White computed NDVI values were derived from QuickBird and WorldView-2 satellite imagery that was captured to coincide with ground-based vegetation cover and spring discharge measurements [3]. Significant linear relationships were established between the image NDVI values and ground-based vegetation cover. Gascon et al. [4] introduced the Sen2Cor processor for the Level-2A product of Sentinel-2 imagery. It converts Top-Of-Atmosphere reflectance (hereinafter referred to as TOA reflectance) to its Bottom-Of-Atmosphere (BOA) counterpart by using the aerosol optical depth (AOD), water vapor content, cirrus cloud correction, terrain correction, and empirical Bidirectional Reflectance Distribution Function (BRDF) corrections. Solórzano et al. [5] used a multispectral image from GeoEye-1 to extract image metrics for modeling a tropical, dry forest based on relative reflectance data that were atmospherically corrected using the Quick Atmospheric Correction (QuAC) algorithm in the Harris Geospatial ENVI software. Miura et al. [6] investigated the cross-sensor compatibility of spectral vegetation indices between VIIRS and MODIS by calculating the vegetation indices, including NDVI, by TOA and TOC reflectance. In the case of Sentinel-2, a project is underway to publicly distribute atmospherically corrected products using the concept of a service platform [7].

Kuhn et al. [8] compared the standard United States Geological Survey (USGS) land surface reflectance products to Landsat-8 and Sentinel-2 aquatic remote sensing reflectance products over several river regions to highlight differences using a correction technique with in situ data. The surface reflectance data supported by the Google Earth Engine (GEE) provide TOA reflectance products from the Landsat Ecosystem Disturbance Adaptive Processing System (LEDAPS) for Landsat 4-5 TM/Landsat 7 ETM+ surface reflectance and the Land Surface Reflectance Code (LaSRC) for Landsat 8 (https://developers.google.com/earthengine/datasets/catalog/LANDSAT_LC08_C01_T1_SR). The surface reflectance products of the Level-1 Precision/Terrain correction for the Landsat 7/8 imagery produced by the absolute atmospheric correction scheme, however, are incomplete due to the limited conditions for product generation. The Sentinel-2 Level-2A surface reflectance products have been available in the Earth Engine data catalog since 2019 (<https://philippgaertner.github.io/2019/04/gee-s2-level-2a-ingestion/>).

To explore the atmospheric corrections of the WorldView-2 image obtained from commercial Earth observation satellites owned by DigitalGlobe, three methods—Simple Linear Regression, Fast Line-of-Sight Atmospheric Analysis of Spectral Hypercubes (FLAASH), and Atmospheric CORrection (ATCOR) models—were evaluated according to in situ reflectance data for particular targets [9]. The mapping of vegetation functional types in urban areas was studied with WorldView-2 imagery [10], and the Normalized Difference Water Index (NDWI) and NDVI values of the WorldView-2 imagery were used for coastline extraction [11]. WorldView-3 satellite image sets are included in the National Land Cover Database (NLCD) for impervious surface area mapping for urban areas [12]. For precision agriculture, the surface reflectance of WorldView-3 was studied by Solano [13] in the process of geographic-object-based image classification for tree crown detection. To evaluate information on tree health in species-rich urban forestry, the potential of the cloud-free Atmospheric Compensation (ACOMP) products of WorldView-3 to mitigate the effects of atmospheric scattering and provide normalized surface reflectance values was investigated [14].

Lee and Lee [15] performed a comparison of products by applying several known atmospheric correction methods with multiple spectral image sets from KOMPSAT-2. KOPMSAT stands for Korea Multi-Purpose Satellite. The results revealed difficulties in generating consistent products,

because atmospheric corrections are affected by several variables. Regarding very high resolution (VHR) KOMPSAT-3/3A images, Kim et al. [16] analyzed the radiative characteristics of KOMPSAT-3 images and experimented to verify the image quality with Landsat-8 images in the same area. Sensor variables for the reflection of the TOA (hereinafter referred to as TOA reflectance) were also presented. Shin et al. [17] conducted a comparative study with both results of the TOA reflectance calculation using KOMPSAT-3A and Landsat 8 OLI images in the test area and reported that the quality of the KOMPSAT-3A images was consistently maintained. In a pilot study on the calibration of KOMPSAT-3/3A images, Yeom et al. [18] performed calculations of TOA reflectance using the second simulation of the satellite signal in the solar spectrum (6S) algorithm, an important radiated transport model, and analyzed the absolute radiometric characteristics of KOMPSAT-3/3A. Ahn et al. [19] produced atmospherically corrected images of Landsat or Sentinel-2 images and used them to propose an adjustment factor for KOMPSAT-3 for TOA reflectance.

Most commercialized tools support extensions or plug-in programs for atmospheric correction; however, most algorithms and methods were developed primarily for MODIS, the Landsat series, and Sentinel-2 images. Thus, as of December 2019, few tools provide atmospheric correction methods that support the sensor model of KOMPSAT-3/3A. It is therefore critical to develop atmospheric correction processing tools for these satellite images to expand the scientific applications of KOMPSAT-3/3A images and other VHR images. Lee and Kim implemented a test version to produce surface reflectance for KOMPSAT-3A based on the open-source Orfeo ToolBox (OTB) environment and performed a case study with KOMPSAT-3A images in the Mekong river area [20].

Based on this test version, this study implemented the OTB extension for KOMPSAT-3A images for an absolute atmospheric correction processing method based on open-source tools as the first step towards establishing an analysis ready data (ARD) database of KOMPSAT images and implementing the actual processing module in the OTB environment. Using this module, experiments were conducted to generate surface reflection with three KOMPSAT 3A images to compare the reflectance results of TOA and TOC with and without the AERONET file, which provides spectral AOD measurements. AERONET is a global aerosol network operated by the National Aeronautics and Space Administration (NASA) and other international satellite missions, which provides the public with different aerosol properties [21]. Moreover, dark object subtraction (DOS)-based atmospheric correction images were prepared and compared with those from the absolute atmospheric correction scheme.

As for NDVI applications for agricultural monitoring purposes, the effects of the atmosphere should be considered because of meaningful results showing a mean difference of 18% between atmospheric and non-atmospheric corrected values [22]. AERONET ground measurements, including aerosol and water vapor parameters, are used as a function of the accuracy of the inputs of the atmospheric correction algorithm to evaluate vegetation indices by TOA or TOC reflectance [23]. Meanwhile, the GEE cloud platform consists of a multi-petabyte analysis-ready data catalog that is co-located with a high-performance, intrinsically parallel computation service. It is accessed and controlled through an internet-accessible application programming interface (API) and an associated web-based interactive development environment (IDE) that enables the rapid prototyping and visualization of results [24]. The GEE provides substantial opportunities for Earth observation and geospatial applications, and it potentially eliminates some of the barriers, particularly in the developing world [25]. Nouri [26] explored the relationship between urban vegetation evapotranspiration (ET) and the vegetation indices derived from newly-developed high spatial resolution WorldView-2 imagery showing that NDVI values were derived for each category of landscape cover, namely, trees, shrubs, turf grasses, impervious pavements, and water bodies.

Based on the background and motivation mentioned above, the first purpose of this study is to address the OTB extension of KOMPSAT-3A images to produce TOA and TOC reflectance by absolute atmospheric correction. The second is to present the difference between the relative atmospheric correction of the DOS scheme and the absolute atmospheric correction for KOMPSAT-3A images through NDVI results. The third is to compare NDVI data from KOMPSAT-3A images with those

obtained using Landsat-8 images in GEE, demonstrating the applicability of surface reflectance data produced from high-resolution multispectral images for future applications.

2. Absolute Atmospheric Correction for Optical Satellite Images and Work Scope

Solar radiation reflected from the surface is detected by satellite sensors through the atmosphere. The radiation energy detected by a satellite sensor is converted to pixel values according to the characteristics of the sensor and provided as an image. The quantity of radiant energy varies greatly from space to time, and it is important to extract accurate measurements from satellite images, regardless of space or time. The pixel values recorded in the image are not uniform across the spectral range, as they are dependent on the season, light and atmospheric conditions, position of the sun, and internal sensor variables. Therefore, calibration for converting pixel values into physical quantities of radiant energy by generalizing the relationship between the radiation energy values recorded in the sensors and the pixel values recorded in the images is an essential process for further analysis.

In addition, applications for crop monitoring or time series analysis related to natural disasters usually involve the comparison of images obtained from different types of sensor or at different times and in different seasons. For this task, physical variables indicating the atmospheric conditions at the acquisition time of the image are used together with a correction factor for the sensor to indicate the amount of physical energy recorded in each sensor. Solar radiation is reflected by various objects and structures on the surface and is detected by sensors in optical satellites, after which it is subjected to atmospheric attenuation that is absorbed and scattered by the Earth's atmosphere; this process affects the pixel values of the image. Therefore, the radiative transfer model is used to quantitatively calculate the amount of radiant energy present. This model requires several physical values containing the position of the satellite at the time of image acquisition as well as the reflective characteristics of the target located on the surface and the condition of the atmosphere at that time. Then, using these variables, a radiation transport model, such as MODTRAN (MODerate resolution atmospheric TRANsmission) or the 6S model, is used for the atmospheric correction of the optical images [27].

The performance of absolute atmospheric corrections for calculating TOC reflectance requires four types of data. The first is the data collected on the ground during the passage of the satellite. The second involves the relative spectral response function curves that indicate the pixel values of the images taken by the satellite, the response level of the sensors, and the sensor gain and offset. The third is the radiation energy values calculated based on the atmospheric conditions and geometrical positions of the sun and sensors required for the selected radiation transport model. The fourth is the measurement data describing atmospheric conditions, such as the AOD, atmospheric pressure, water vapor volume, ozone volume, and composition and quantity of aerosol gases.

Atmospheric correction is not necessary for all land applications of satellite images; however, it is an important process for the physical analysis of land properties or time series image analysis, such as the detection of change in the environment. There are several algorithms based on MODTRAN and the 6S model for this correction: ACORN (Atmospheric CORrection Now), FLAASH, ATREM (ATmospheric REMoval), and ATCOR. In addition to commercial tools, Bunting [28] developed the Atmospheric and Radiometric Correction of Satellite Imagery (ARCSI) tool using the 6S model; this model supports Landsat, SPOT, Sentinel-2, Rapideye, WorldView, and Pleiades. Franz et al. [29] developed a tool called the Framework for Operational Radiometric Correction for Environmental Monitoring (FORCE) that can produce Landsat ARD by applying a water vapor dataset using the MODIS image. Leutner [30] developed RSToolbox, an open-source package for providing relative atmospheric correction processing according to the DOS algorithm for Landsat images in the R environment. In the SNAP Toolbox, a plug-in method of the iCOR atmospheric correction tool [31] is mainly used for Sentinel 2 and Landsat 8 images. The TOA reflection tool in SAGA [32] utilizes a module using the DOS scheme named `i.landsat.toar` in the GRASS library for Landsat images only.

Figure 1 shows the types of optical satellite images and the spatial resolution of multispectral bands, swath width at the nadir, and atmospheric corrections for producing surface reflectance. The spectral

band specification of KOMPSAT-3A is as follows: 450–900 μm for the panchromatic band, 450–520 μm for MS1 (blue), 520–600 μm for MS2 (green), 630–690 μm for MS3 (red), and 760–900 μm for MS4 (near infrared: NIR). The ground sample distance (GSD) at the nadir is 0.55 m for a panchromatic image, 2.2 m for multispectral bands, and 5.5 m for near infrared data. The radiometric resolution of data quantization is 14 bits. The swath width of KOMPSAT 3A is 12 km, and it is 15.4 times narrower than that of Landsat-8 OLI. Meanwhile, KOMPSAT-3 has the same spectral band specifications as KOMPSAT 3A, but the GSD for a panchromatic image and multispectral bands in the swath width of 15 km at the nadir is 0.7 m and 2.8 m, respectively. As for the four multi-spectral bands of DigitalGlobe WorldView-4 with a sensor resolution of 1.24 m and a swath width of 13.2 Km at the nadir, the wavelength widths for the blue band, green band, red band, and near infrared band are 450–510, 510–580, 655–690, and 780–920 μm , respectively. The panchromatic band with a spatial resolution of 0.31 m at the nadir has a wavelength width of 450–800 μm (<https://www.satimagingcorp.com/satellite-sensors/geoeye-2/>). DigitalGlobe provides commercialized image products by AComp that support three radiometric correction methods: TOA reflectance, Rayleigh-only reflectance, and surface reflectance [33]. Among them, surface reflectance compensates for atmospheric absorption and scattering phenomena and approximates what would be measured by a sensor held just above the surface without any alterations from the atmosphere. Of these three reflectance products, surface reflectance can be used for many kinds of application such as land use and cover analysis, time series evaluation, feature extraction, spectral matching, tonal balancing, and spectral accuracy evaluation.

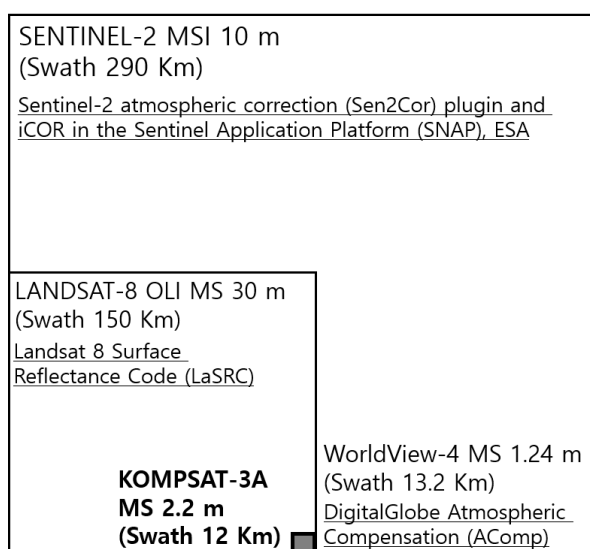


Figure 1. Optical satellite images: the spatial resolution of multispectral bands, swath width at the nadir, and atmospheric correction for producing surface reflectance.

Figure 2 summarizes the workflow of this study. The OTB tool applied in this study was the OTB extension embedded in the sensor model, solar irradiation, and the relative spectral response function required for the atmospheric calibration of KOMPSAT-3A. An extension in a piece of software is a type of computer program that is meant to extend or add to what the base program is able to do. The tool implemented in this study is called OTB extension for KOMPSAT-3A, and it was rebuilt in the OTB environment, rather than being a plug-in inserted into it. This tool automatically reads input variables for atmospheric calibration from the images and applies them to produce TOA and TOC reflectance. Therefore, the entire source must be rebuilt, rather than simply being inserted.

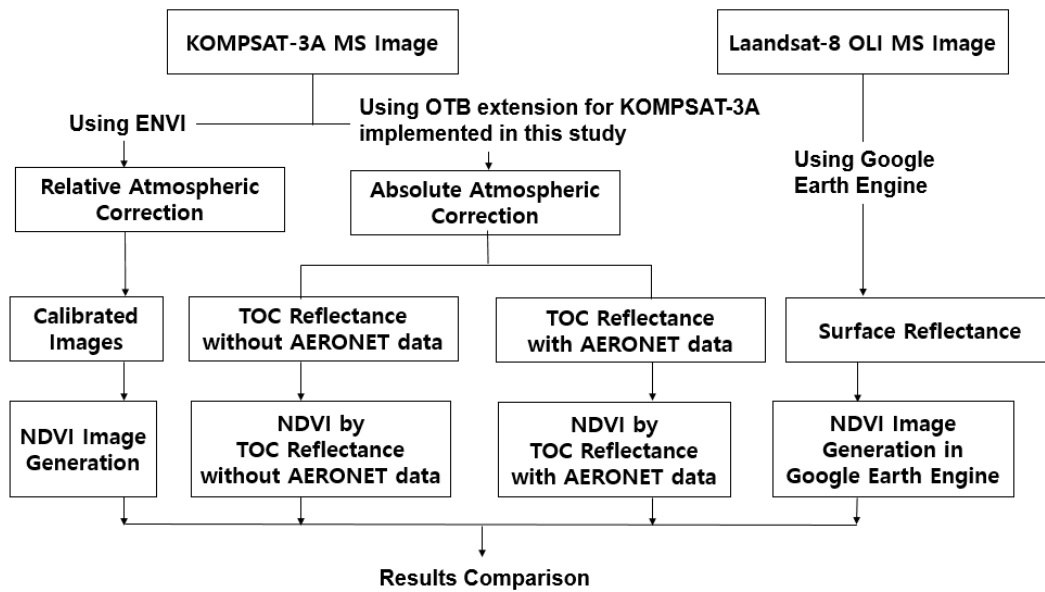


Figure 2. The workflow of this study and datasets used. The notation TOA, TOC, and NDVI mean Top-of-Atmosphere, Top-of-Canopy, and normalized difference vegetation index, respectively.

3. Applied Scheme and Data

3.1. Atmospheric Correction Module in the Orfeo ToolBox (OTB): OTB Extension for KOMPSAT-3A

In this study, the absolute atmospheric correction processing function for KOMPSAT-3A was performed using OTB extension for KOMPSAT-3A, as a newly implemented module in the OTB environment, as illustrated in Figure 3.

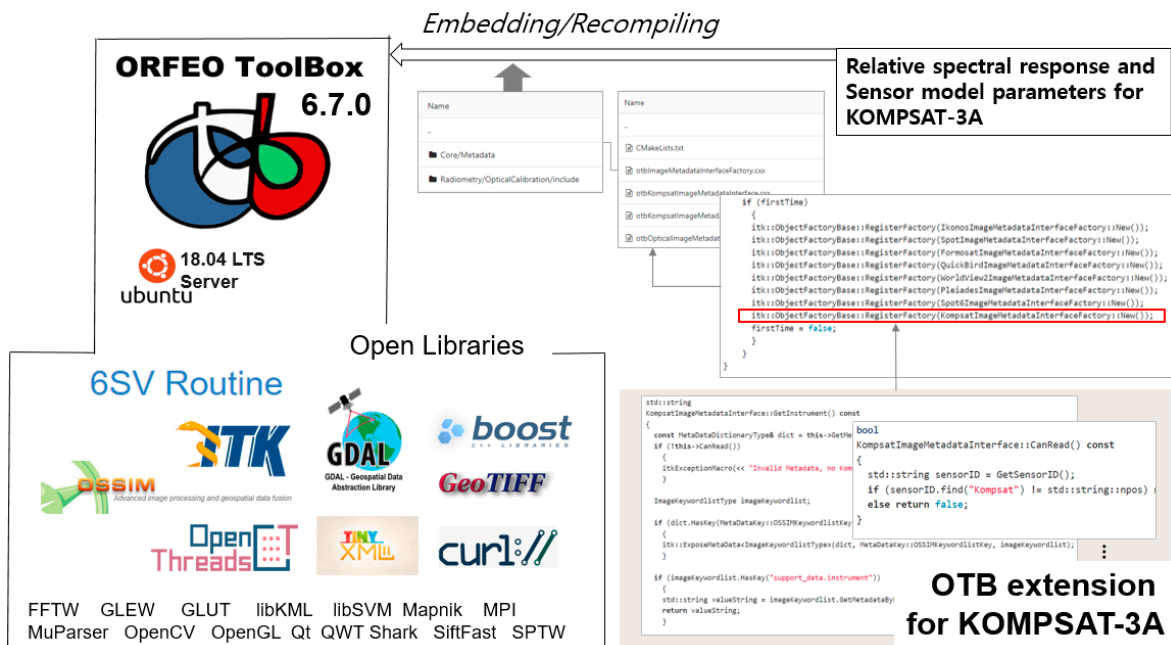


Figure 3. The recompiling process for the Orfeo ToolBox (OTB), its external libraries, and OTB extension for KOMPSAT-3A on Ubuntu. Modified from [20].

The OTB is an open-source product for remote sensing that includes a fast image viewer, apps callable from various programming languages or external platforms such as Python or QGIS, and a C++ application programming interface (API) [34]. Since 2015, this product has been managed and

developed by the Open-Source GeoSpatial Foundation (OSGeo), a non-profit and non-governmental organization. Modules applied to KOMPSAT-3A can also be applied to KOMPSAT-3 because both sensor models have the same specifications, including the wavelength range and spectral response for each band. Furthermore, data of the atmospheric conditions for calculating TOC reflectance are available in the AERONET database. AERONET is a global aerosol network operated by NASA and other international satellite missions, which provides the public with different aerosol properties. It involves the AOD, which indicates the transparency of the atmosphere measured using solar photometric observations and satellite images at 1038 measurement stations located around the world (<https://aeronet.gsfc.nasa.gov/>). The AERONET data used in this study are monthly data for the imagery acquisition period. When the AERONET data are read from the OTB, the first step is to search the date column and retrieve the image acquisition date, month, and year. Then, the values are stored with all data within an hour of the predefined date, with error ranges calculated as mean values to update parameters, such as the amount of water vapor and aerosol property values, which are required for the TOC reflectance calculation.

Under an Apache 2.0 license, the OTB uses many external open-source systems, such as the Insight Toolkit (ITK), Geospatial Data Abstraction Library (GDAL), OSSIM, libSVM, OpenCV, and Shark, with a 6SV routine [35] for the 6S model [36]. The 6S model is a radiation transport model that is designed to simulate the reflection of solar radiation by atmospheric surface systems combined in a wide range of atmospheric, spectral, and geometrical conditions, with inputs of altitude, atmospheric pressure, temperature, moisture density, ozone density, water content, and ozone concentrations. The OTB supports the atmospheric calibration processing module using the 6S model for limited sensors, such as QuickBird, IKONOS, WorldView-2, FORMOSAT, Pleiades, and SPOT, and does not support KOMPSAT-3A images. Therefore, to generate the reflectance of TOA and TOC for KOMPSAT-3A, separate source code or scripts must be implemented to handle the model variables of the sensor or the physical values used for atmospheric correction, and they must be compiled with the OTB engine.

The following is a formula that is used to determine the reflectance of TOA and TOC according to atmospheric correction for a KOMPSAT-3A image:

$$L_{\lambda} = Gain \times (DN) + Offset \quad (1)$$

where L_{λ} is the spectral radiance of the wavelength, *Gain* and *Offset* are the sensor's characteristics, and *DN* is the digital number. The sensor radiation of the band wavelength of KOMPSAT 3A uses the data given in the TOA radiance reflection conversion [37].

$$\rho_{\lambda,TOA} = \frac{\pi L_{\lambda} d^2}{(ESUN_{\lambda}) \cos \theta_s} \quad (2)$$

where ρ_{λ} represents the TOA reflectance on the satellite image band wavelength, d is the Earth–sun distance, $ESUN_{\lambda}$ is the solar exoatmospheric irradiance, and θ_s is the solar zenith angle [38].

$$\rho_{TOC} = \frac{\frac{\rho_{TOA} - \rho_{atm}}{T(\mu_s)T(\mu_{\gamma})t_g}}{1 + S \frac{\rho_{TOA} - \rho_{atm}}{T(\mu_s)T(\mu_{\gamma})t_g}} \quad (3)$$

Here, ρ_{TOC} , ρ_{TOA} , and ρ_{atm} represent the reflectance of TOC, TOA, and intrinsic atmospheric reflectance, respectively. S is a correction constant, and $T(\mu_s)$, $T(\mu_{\gamma})$, and t_g represent downward transmittance, upward transmittance, and the albedo of the atmosphere, respectively [39].

TOA reflectance is obtained by taking the sensor gain and offset, solar irradiance, and spectral response levels into account. In addition to the information used to calculate TOA reflectance, the calculation of TOC reflectance also requires information about the optical thickness of the atmosphere, atmospheric pressure, water vapor volume, ozone volume, and composition and quantity of aerosol gases.

The sensor information registered in the OTB environment is used for calibration processing through the automatic parsing of the required factor values, such as the day, bias, gain, azimuth, and other information by reading the same GEOM file name for each band. For the automatic input of these values, only sensors registered with the OTB are allowed. The GEOM file is a form of image metadata storage format used by the OSSIM remote sensing library (<https://sourceforge.net/projects/ossim/>) that is used inside the OTB. In this study, OTB core metadata were added for KOMPSAT-3A images, and a script for generating GEOM files was developed so that input values could be applied immediately during OTB calibration processing.

Figure 4 presents the solar irradiance in the range used in KOMPSAT-3A atmospheric correction as well as the relative spectral response data for the KOMPSAT-3A band. The solar spectral irradiance was based on the American Society for Testing and Materials (ASTM) G-173 data [40]. In addition, data of the atmospheric conditions for calculating TOC reflectance are available in the AERONET database (https://aeronet.gsfc.nasa.gov/cgi-bin/type_piece_of_map_cloud). AERONET is a global aerosol network operated by NASA and other international satellite missions that provides the public with various aerosol properties, such as AOD, which indicates the transparency of the atmosphere measured using solar photometric observations and satellite images at ground stations located around the world. The AERONET file provides three levels of data depending on the processing level of the data. Level 1 contains raw data, Level 1.5 contains data in which the effects of clouds are eliminated, and Level 2 contains the most accurate data whose quality is guaranteed through a calibration process. The two physical quantities presented in Figure 4 are included in the OTB compilation for the new implementation for extracting the TOC reflectance of KOMPSAT-3A.

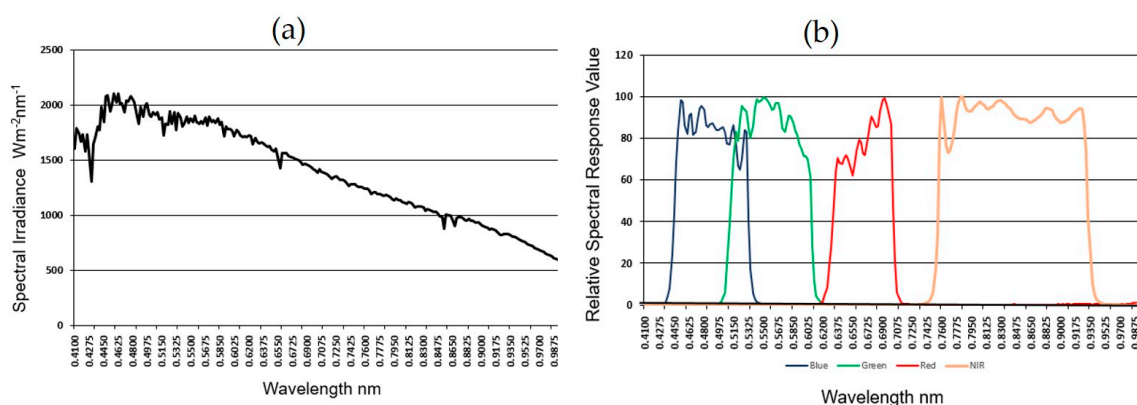


Figure 4. (a) Solar spectral irradiance based on ASTM G-173 [40] and (b) the relative spectral response of KOMPSAT-3A [16].

3.2. KOMPSAT-3A and Landsat Data for NDVI Calculation

In this study, we utilized KOMPSAT-3A images of Canberra, Australia, as shown in Figure 4, and conducted some experiments related to NDVI computation.

This study involved a test experiment with data from a single image. Although it is really necessary to use a large number of image datasets for different climate environments or to address a mosaicked image of multiple images in a wide area, this study did not focus on the detailed interpretation of a certain region or the performance analysis of a development tool at this stage. We plan to address these areas in the next stage in terms of urban forest applications.

Among the algorithms and schemes used for atmospheric correction to extract surface reflectance, the DOS method, implemented in the ENVI software, is simple and effective. The DOS is a relative atmospheric correction scheme that eliminates the effects of atmospheric factors from a target image by subtracting a pixel value representing the band minimum as an average based on a region of interest (ROI) specified by users, from each band. The DOS-based NDVI was selected for comparison with a TOC-based scheme. The reason for adopting this method as the comparison scheme was the absence of

a proprietary tool or open-source software for generating TOC reflectance using the physical properties of the KOMPSAT-3A sensor model. This is because it involves the removal of haze effects without usage. Most schemes that are designed to obtain surface reflectance data using physical parameters are suitable for Landsat or Sentinel-2 imagery. For DOS processing, users select dark objects for each image by a rather heuristically subjective criterion, without considering atmospheric parameters such as the AOD, water vapor, or atmospheric pressure provided by the AERONET data.

Figure 5 shows the data coverage of the study area in the Canberra region, Australia, with the AERONET measurement station located centrally in the image. The newly implemented module was applied to produce TOC reflectance data for the image. In this module, the input parameters for generating TOC reflectance, such as the solar distance, solar azimuth angle, solar elevation angle, and viewing angle, are automatically read and processed with the acquisition date and time of image collection as well as the auxiliary metadata file in the KOMPSAT-3A bundle datasets. The sensor model data of KOMPSAT-3A, including the gain and bias, relative spectral response data of each band, and spectral irradiance data, are also incorporated. The OTB allows choice items for the non-aerosol model and continental, maritime, urban, or desert data for the aerosol model to be selected for the 6S radiative transfer model, according to the applied area types. In addition, many physical parameters for TOC processing are needed, including the ozone level, quantity of water vapor, atmospheric pressure, and AOD.

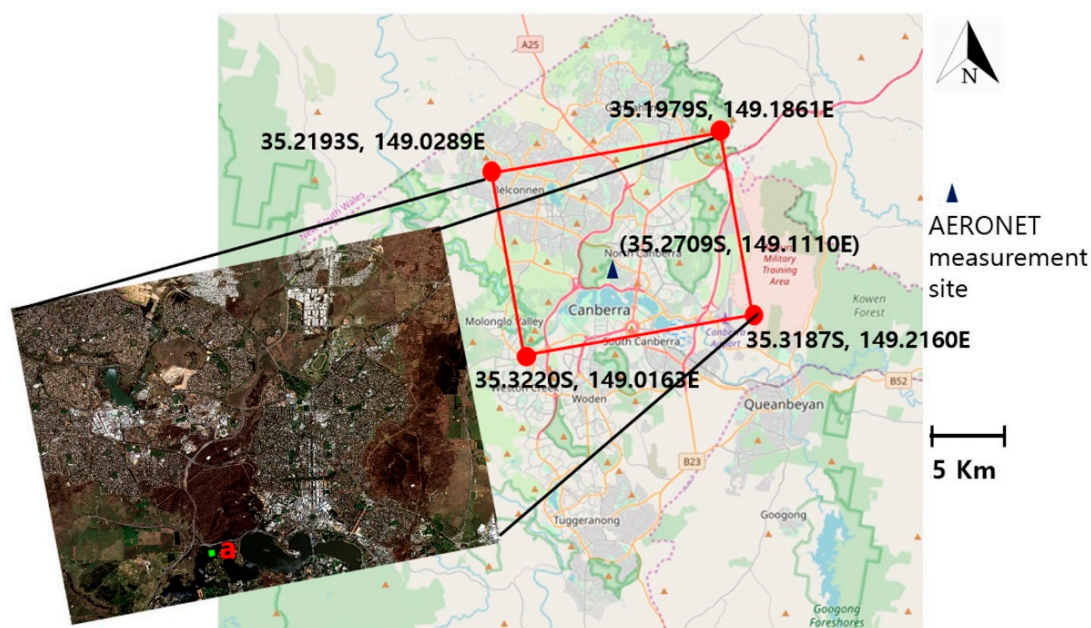


Figure 5. Canberra region, Australia, covered by KOMPSAT-3A (7 February 2016) and a measurement station point for the AERONET data.

There are many types of radiometric indices extraction function in the OTB feature extraction feature, including the NDVI, RVI (Ratio Vegetation Index), and IPVI (Infrared Percentage Vegetation Index). In this study, the NDVI processing of TOC and DOS results for the KOMPSAT-3A image was handled using the OTB NDVI function.

For comparison with the surface reflectance of Landsat-8 covering the same area, the GEE NDVI API [41] was also used for NDVI computation processing.

The GEE portal provides enhanced opportunities for undertaking Earth observation studies. Established towards the end of 2010, the cloud platform provides access to over 500 types of satellite and other ancillary data and contains algorithms that can process large amounts of data with relative ease. Overall, the GEE has introduced a new big data paradigm for the storage and analysis of remotely sensed data at a scale that is not feasible using desktop processing machines. The GEE provides a

Landsat-8 surface reflectance tier 1 dataset [42] according to Landsat ARD guidelines [43]. The GEE is a PaaS-type cloud service that enables simple image processing with real-time scripting. PaaS stands for platform-as-a-service, a type of cloud service. A part of a script code for NDVI computation is shown in Figure 6. The ImageCollection function in the GEE allows users to search the data provided on a desired date and process it directly through the normalized differential function among the image processing algorithms. Two Landsat-8 images were searched using the filterDate method in the GEE that were captured on 6 February 2016 and 13 February 2016. For a comparison with the KOMPSAT-3A image, the image taken on 6 February 2016 that was chosen by the first method was used.



```

1 var imageCollectionLandsat8_Tier1 = ee.ImageCollection("LANDSAT/LC08/C01/T1_SR");
2 var point = new ee.Geometry.Point(149.10801273294805, -35.30130219146685);
3 var calNDVI = function (image){
4   return image.normalizedDifference(['B5', 'B4']);
5 }
6 var area1 = ee.Geometry.Polygon([
7   [149.012818410779, -35.18184994777987]
8   ,[149.21226222593359, -35.178369838395774]
9   ,[149.21607978309225, -35.31871456363667]
10  ,[149.01629239689703, -35.32221269913508]
11  ]);
12 Map.setCenter(149.11, -35.30, 8);
13 var landsatTier1 = ee.Image(imageCollectionLandsat8_Tier1.filterDate('2016-02-01', '2016-02-20')
14   .filterBounds(point).sort('CLOUD_COVER').first().clip(area1));
15 var resultNDVI = calNDVI(landsatTier1);
16 var palette = {min:-1.0, max: 1.0, palette: '00078c, 0042f1, 0daafa, 5affa5, cce739, ff8400, 950800'};
17 Map.addLayer(resultNDVI, palette, 'TOC NDVI');
18
19 Export.image.toDrive({
20   image : resultNDVI,
21   description : 'TOC_NDVI',
22   fileFormat: 'GeoTIFF',
23   scale : 30,
24   maxPixels: 314758288
25 });

```

Figure 6. Script for NDVI processing in the Canberra region, Australia, covered by Landsat-8 OLI (6 February 2016) in the Google Earth Engine code editor.

4. Results and Discussion

Absolute atmospheric correction for high-resolution satellite images is a very important subject in terms of the value-added uses of images such as the commercial WorldView series, besides KOMPSAT-3A, and it is also important in terms of the quality control of the satellite images concerning calibration and validation. Its demand continues to grow due to the advent of new multi-spectral high-resolution images from the private and public sectors. The TOA and TOC reflection images are important products obtained from the absolute atmospheric correction of satellite images. However, most proprietary software does not provide an absolute atmospheric correction module for all kinds of high-resolution image, so relative atmospheric correction such as the DOS scheme is inevitable when users want to use a certain specific sensor image in their applications.

Although NDVI, which was applied in this study, is a simple computation method, the results vary widely depending on the data used. Absolute atmospheric correction produces a constant result, whereas relative atmospheric corrections could be inconsistent because the input values may vary. In addition, absolute atmospheric correction can standardize the processing procedures, but with relative atmospheric corrections, the results can be affected by the user's experience and understanding level in terms of multi-spectral bands.

Figure 7 shows four cases of NDVI computation: the difference among Landsat-8 surface reflectance tier 1 in the GEE, the DOS-based reflectance produced with the ROI designated as "a" in the image in Figure 5, and two TOC reflectance results obtained using the OTB extension for KOMPSAT-3A.

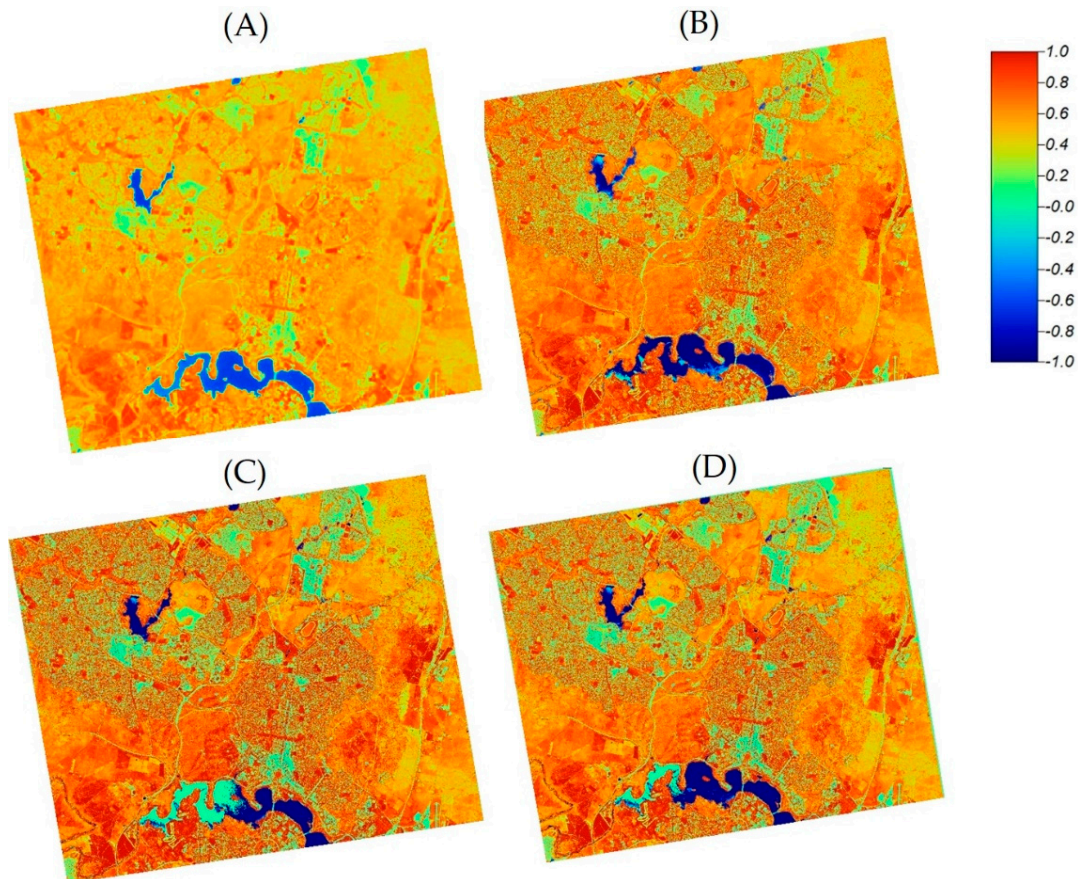


Figure 7. The NDVI results using red and near infrared (NIR) bands: (A) the Landsat-8 surface reflectance tier 1 in the Google Earth Engine (465×379), (B) the dark object subtraction (DOS)-based reflectance (6351×5171) of KOMPSAT-3A, (C) the TOC reflectance without the AERONET data (6351×5171) of KOMPSAT-3A, and (D) the TOC reflectance with the AERONET data (6351×5171) of KOMPSAT-3A.

Figure 7A shows the resultant image from the GEE. This result of Landsat-8 OLI is quite different from other cases of KOMPSAT-3A. The Landsat-8 surface reflectance tier 1 of the GEE was generated from LaSRC by the USGS, whereas the TOC reflectance of KOMPSAT-3A was taken from the OTB extension. The DOS method often sets the ROI using subjective experience, so the results may vary depending on which region is selected, which is a relative atmospheric correction. The NDVI was conducted using DOS-based and TOC reflectance data, as displayed in Figure 7B. Because the sensor resolution differs between Landsat and KOMPSAT-3A, the number of pixels is not identical. The number of pixels in Figure 7A is 465×379 , and that of other the results shown in Figure 7B–D is 6351×5171 .

For TOC reflectance, the two datasets shown in Figure 7C,D were applied for NDVI calculation. Figure 7C exhibits the results obtained using the red and near infrared bands of TOC reflectance without the AERONET data, while Figure 7D shows the TOC reflectance with the AERONET data. This experiment was performed because AERONET observation stations are not always within the coverage range of imagery. In the module implemented for generating TOC reflectance, it is not a mandatory input dataset. The distinguishing features among the three products were revealed by visual interpretation in the range of $[-1,1]$. The negative values close to -1.0 in NDVI correspond to water bodies, while values from -0.1 to 0.1 (close to zero) are generally interpreted as barren areas.

Low positive values represent shrubs and grassland regions, whereas high positive values approaching $+1.0$ reflect temperate and tropical forests. To represent these features analytically, the results were partitioned into three ranges, namely, -1.0 to 0.1 , 0.1 to 0.6 , and 0.6 to 1.0 , by a density

slicing scheme, as shown in Figure 7. Density slicing is a reclassification scheme where a raster image with continuous values is converted into a series of intervals, slices, or classes, and different colors are assigned to each slice or class as group variations with their legend.

The comparison results of the NDVI of four classes are represented by density slicing with a percentage of the number of pixels in each class. Figure 8A is the result of Landsat-8 surface reflectance tier 1 in the GEE. Figure 8B–D show DOS-based reflectance, TOC reflectance without the AERONET data, and TOC reflectance with the AERONET data, respectively. These results are more clearly indicative of the differences, compared to the results shown in Figure 7. In particular, visual interpretation shows that the distribution of Figure 8A, which is concentrated in the middle class in range 0.1 to 0.6, is different from that of the other three cases, which represent the high vegetated trend over 0.6. In detail, the results of the DOS-based corrections are different from those of the TOC-based scheme. Furthermore, the processing results of TOC reflection with or without the AERONET data differ, showing the same proportion at the low class of -1.0 to 0.1 , but reveal a difference of approximately ± 4.5 percentage points in the upper two classes. This extension treats the use of the AERONET data as optional. In some cases, these data may not be applicable and may not be influenced when those of the AERONET measurement site which is far away are used. This case study showed that the application of these data affects the results. The suitability of the results for NDVI can be verified by experimenting with in situ data in the study area.

The GEE is an easy-to-handle tool for obtaining wide-area NDVI, but it is not suitable for precise analyses, such as analysis of urban forestry, because the data used are medium-resolution. To date, there has been no example of the ARD building of high-resolution images such as the WorldView series. The Committee on Earth Observation Satellites (CEOS) established the concept of CEOS Analysis Ready Data for Land (CARD4L) product types and their framework, to be content with the practical demand for such satellite data [44]. However, it does not provide the ARD guidelines for producers and users of high-resolution EO images yet. The USGS established a Landsat ARD database containing data of different levels in the Earth Explorer [45] to make it possible to use satellite images for monitoring or time series landscape analysis purposes without having to perform calibration or pre-processing. This Landsat ARD database partitions the territory of a country into a constant grid structure associated with a projection coordinate system and provides surface reflection images using atmospheric correction. The ARD products are time-series stacks of EO imagery prepared for a user to apply without pre-processing the image data. Therefore, for NDVI results at the regional scale, it is possible to perform pre-processing on an individual image and then aggregate the data into a mosaic image covering that region. It is necessary to calculate other vegetation indices as well as NDVI and estimate the results, since this is the first NDVI result using the TOC reflectance of a KOMPSAT-3A image.

The use of AERONET data as the input data for TOC reflectance computation was expected to be important for the results. This study shows this effect through NDVI calculations. The NDVI is a quantitative index with a high actual utilization value, although it is calculated by a simple formula using the red and near infrared bands. It needs to analyze the difference between the blue and green bands. To apply high-resolution satellite images to big data or deep learning, high performance processing for a huge dataset volume is the main topic, but it is also important to analyze the applicability and suitability of individually pre-processed data. The next step of this work is to compute the Atmospherically Resistant Vegetation Index (ARVI) [46] using three bands—red, near infrared, and blue—to discover other aspects and effects of high-resolution multispectral bands for absolute atmospheric corrections.

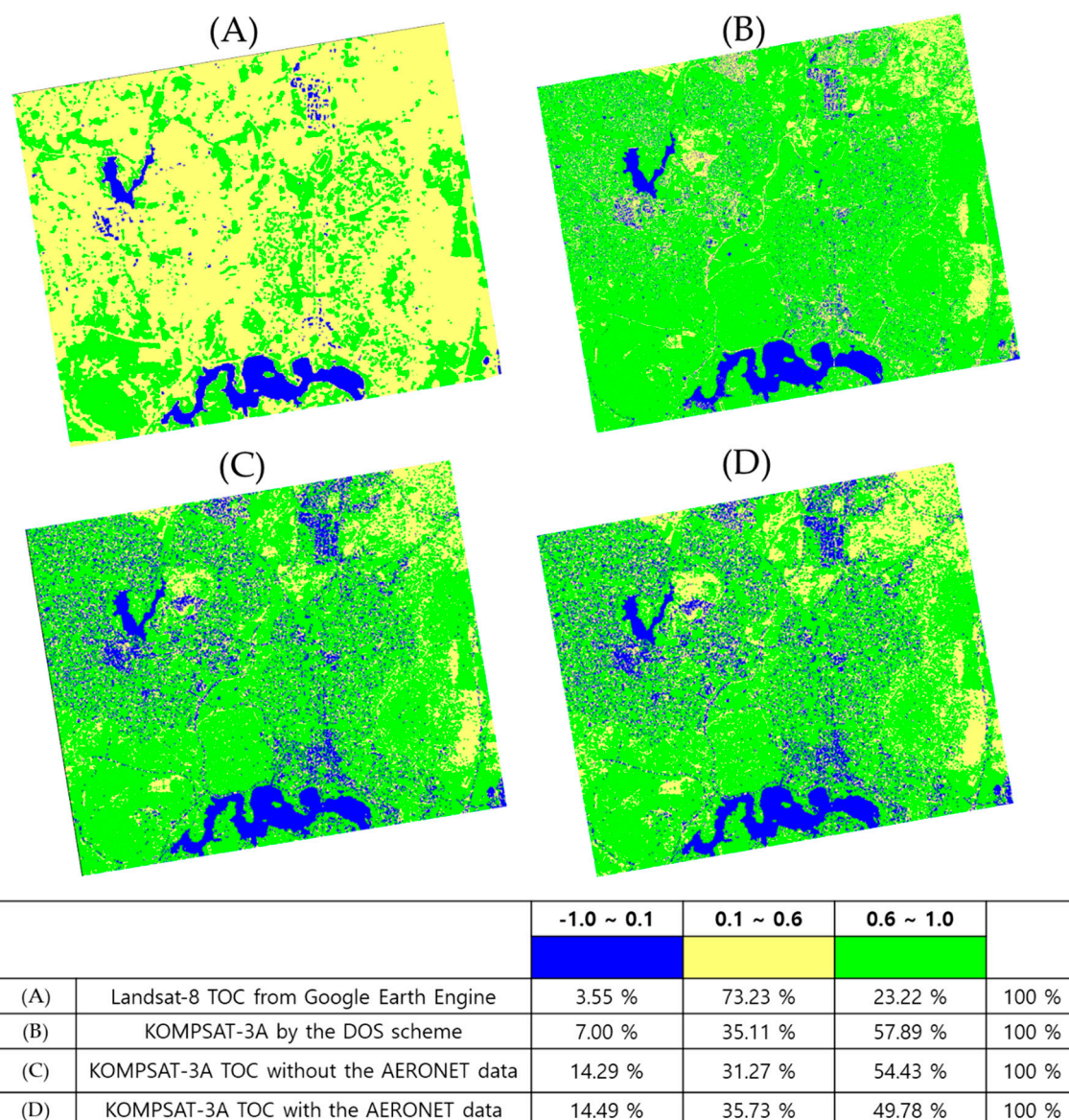


Figure 8. Comparison of the NDVI results of three classes by density slicing: (A) Landsat-8 surface reflectance tier 1 in the Google Earth Engine, (B) DOS-based reflectance, (C) TOC reflectance without the AERONET data, and (D) TOC reflectance with the AERONET data.

5. Conclusions

Although atmospheric correction is a classic subject of research in satellite remote sensing, it is still being researched and developed, because of its practical importance in increasing the value of data. The surface reflection result is an important product obtained from the absolute atmospheric correction of satellite images. These data are important for establishing an ARD database. However, tools to extract TOC reflectance data from KOMPSAT-3A images are unavailable. For these functions, open-source tools are yet to be developed or published. In this study, an atmospheric correction extension module in OTB open-source software was implemented. Treating an important pre-processing function, absolute atmospheric correction, as open-source provides a huge economic advantage in terms of the large volume of high-resolution satellite image processing possible, because a base engine software can be customized in the way the developers and operators want it to be. For other high-resolution satellite sensor models, OTB extensions are also possible.

The NDVI results of this study are the first example computed using the surface reflectance obtained from the absolute atmospheric correction of a KOMPSAT-3A image. Therefore, quantitative comparative studies with different sensors or conditions are required. This study focused on the results of the use of AERONET data, among many cases. The NDVI results using TOC reflectance with or without AERONET data were considerably different from those obtained with the DOS scheme, a kind of relative atmospheric correction, and the Landsat-8 surface reflectance of the GEE. The GEE NDVI result was generated at different resolutions and with different applied algorithms, compared with KOMPSAT-3A. If AERONET data are available for the target area, then the aerosol data file is read directly in the newly implemented module. Although it was demonstrated that AERONET data are optional for NDVI evaluation, the results were affected by the inclusion of the data. The TOC reflectance results with the AERONET data containing atmospheric physical variables are considered to be more practical estimates compared with those obtained from relative methods or those lacking physical variables. Further experiments on various quantitative vegetation indices such as the ARVI using TOC reflectance will be conducted in future studies. It is expected that the need for computerized schemes to extract surface reflectance data will likely increase because of the practical demand for precise analyses using high-resolution multispectral images.

Author Contributions: Conceptualization, Kiwon Lee, Yongseung Kim; Methodology, Kiwon Lee, Kwangseob Kim; Software, Kwangseob Kim, Kiwon Lee; Data Curation and Validation, Yongseung Kim, Sun-Gu Lee; Investigation and Analysis, Kiwon Lee; Writing, Kiwon Lee; All authors have read and agreed to the published version of the manuscript.

Funding: This research was funded by the National Land Space Information Research Program from the Ministry of Land, Infrastructure, and Transport, Korea grant number [14NSIP-B080144-01] to Kwangseob Kim and the International Cooperation Promotion Study for K-GEO Role Enhancement (2019) grant to Sun-Gu Lee and Yongseung Kim. This research was financially supported by Hansung University for Kiwon Lee.

Acknowledgments: The authors thank the anonymous reviewers for their careful reading of our manuscript and their many insightful comments, corrections and suggestions.

Conflicts of Interest: The authors declare no conflicts of interest.

References

1. Horion, S.; Fensholt, R.; Tagesson, T.; Ehammer, A. Using earth observation- based dry season NDVI trends for assessment of changes in tree cover in the Sahel. *Int. J. Remote Sens.* **2014**, *35*, 2493–2515. [[CrossRef](#)]
2. Fan, X.; Liu, Y. A global study of NDVI difference among moderate-resolution satellite sensors. *ISPRS J. Photogramm.* **2016**, *121*, 177–191. [[CrossRef](#)]
3. White, D.C.; Lewis, M.M.; Green, G.; Gotch, T.B. A generalizable NDVI based wetland delineation indicator for remote monitoring of groundwater flows in the Australian Great Artesian Basin. *Ecol. Indic.* **2016**, *60*, 1309–1320. [[CrossRef](#)]
4. Gascon, F.; Bouzinac, C.; Thépaut, O.; Jung, M.; Francesconi, B.; Louis, J.; Lonjou, V.; Lafrance, B.; Massera, S.; Gaudel-Vacaresse, A.; et al. Copernicus Sentinel-2A Calibration and Products Validation Status. *Remote Sens.* **2017**, *9*, 584. [[CrossRef](#)]
5. Solórzano, J.V.; Meave, J.A.; Gallardo-Cruz, J.A.; González, E.J.; Hernández- Stefanoni, J.L. Predicting old-growth tropical forest attributes from very high resolution (VHR)-derived surface metrics. *Int. J. Remote Sens.* **2017**, *38*, 492–513. [[CrossRef](#)]
6. Miura, T.; Muratsuchi, J.; Vargas, M. Assessment of cross-sensor vegetation index compatibility between VIIRS and MODIS using near-coincident observations. *J. Appl. Remote Sens.* **2018**, *12*, 045004. [[CrossRef](#)]
7. Vuolo, F.; Zoltak, M.; Pipitone, C.; Zappa, L.; Wenng, H.; Immitzer, M.; Weiss, M.; Baret, F.; Atzberger, C. Data Service Platform for Sentinel-2 Surface Reflectance and Value-Added Products: System Use and Examples. *Remote Sens.* **2016**, *8*, 938. [[CrossRef](#)]
8. Kuhn, C.; de Matos Valerio, A.; Ward, N.; Loken, L.; Sawakuchi, H.O.; Kampel, M.; Richey, J.; Stadler, P.; Crawford, J.; Striegl, R.; et al. Performance of Landsat-8 and Sentinel-2 surface reflectance products for river remote sensing retrievals of chlorophyll-a and turbidity. *Remote Sens. Environ.* **2019**, *224*, 104–118. [[CrossRef](#)]

9. Manakos, I.; Manevski, K.; Kalaitzidis, C.; Edler, D. Comparison between Atmospheric Correction Modules on the Basis of Worldview-2 Imagery and In Situ Spectroradiometric Measurements. In Proceedings of the 7th EARSeL SIG Imaging Spectroscopy workshop, Edinburgh, UK, 11–13 April 2011.
10. Maglione, P.; Parente, C.; Vallario, A. Coastline extraction using high resolution WorldView-2 satellite imagery. *Eur. J. Remote Sens.* **2014**, *47*, 685–699. [[CrossRef](#)]
11. Yan, J.; Zhou, W.; Han, L.; Yuguo Qian, Y. Mapping vegetation functional types in urban areas with WorldView-2 imagery: Integrating object-based classification with phenology. *Urban For. Urban Gree.* **2018**, *31*, 230–240. [[CrossRef](#)]
12. Xian, G.; Shi, H.; Dewitz, J.; Wu, Z. Performances of WorldView 3, Sentinel 2, and Landsat 8 data in mapping impervious surface. *Remote Sens. Appl. Soc. Environ.* **2019**, *15*, 100246. [[CrossRef](#)]
13. Solano, F.; Fazio, S.D.; Modica, G. A methodology based on GEOBIA and WorldView-3 imagery to derive vegetation indices at tree crown detail in olive orchards. *Int. J. Appl. Earth Obs.* **2019**, *83*, 101912. [[CrossRef](#)]
14. Fang, F.; McNeil, B.; Warner, T.; Dahle, G.; Eutsler, E. Street tree health from space? An evaluation using WorldView-3 data and the Washington D.C. Street Tree Spatial Database. *Urban For. Urban Gree.* **2020**, *49*, 126634. [[CrossRef](#)]
15. Lee, H.-S.; Lee, K.-S. Atmospheric Correction Problems with Multi-Temporal High Spatial Resolution Images from Different Satellite Sensors. *Korean J. Remote Sens.* **2015**, *31*, 321–330, (In Korean with English abstract). [[CrossRef](#)]
16. Kim, J.; Jin, C.; Choi, C.; Ahn, H. Radiometric characterization and validation for the KOMPSAT-3 sensor. *Remote Sens. Lett.* **2015**, *6*, 529–538. [[CrossRef](#)]
17. Shin, D.Y.; Ahn, H.Y.; Lee, S.G.; Choi, C.U.; Kim, J.S. Radiometric Cross-calibration of KOMPSAT-3A with Landsat-8. In Proceedings of the International Archives of the Photogrammetry, Remote Sensing and Spatial Information Sciences, Volume XLI-B1, 2016, XXIII ISPRS Congress, Prague, Czech Republic, 12–19 July 2016.
18. Yeom, J.M.; Ko, J.; Hwang, J.; Lee, C.S.; Choi, C.U.; Jeong, S. Updating Absolute Radiometric Characteristics for KOMPSAT-3 and KOMPSAT-3A Multispectral Imaging Sensors Using Well-Characterized Pseudo-Invariant Tarps and Microtops II. *Remote Sens.* **2018**, *10*, 697. [[CrossRef](#)]
19. Ahn, H.Y.; Kim, K.Y.; Lee, K.D.; Park, C.W.; So, K.H.; Na, S.I. Feasibility Assessment of Spectral Band Adjustment Factor of KOMPSAT-3 for Agriculture Remote Sensing. *Korean J. Remote Sens.* **2018**, *34*, 1369–1382, (In Korean with English abstract). [[CrossRef](#)]
20. Lee, K.; Kim, K. An Experiment for Surface Reflectance Image Generation of KOMPSAT 3A Image Data by Open Source Implementation. *Korean J. Remote Sens.* **2019**, *35*, 1327–1339, (In Korean with English abstract). [[CrossRef](#)]
21. AERONET, Aerosol Robotic Network. Available online: <https://aeronet.gsfc.nasa.gov/> (accessed on 10 January 2020).
22. Hadjimitsis, D.G.; Papadavid, G.; Agapiou, A.; Themistocleous, K.; Hadjimitsis, M.G.; Retalis, A.; Michaelides, S.; Chrysoulakis, N.; Toullos, L.; Clayton, C.R.I. Atmospheric correction for satellite remotely sensed data intended for agricultural applications: Impact on vegetation indices. *Nat. Hazards Earth Syst. Sci.* **2010**, *10*, 89–95. [[CrossRef](#)]
23. Shabanov, N.; Vargas, M.; Miura, T.; Sei, A.; Danial, A. Evaluation of the performance of Suomi NPP VIIRS top of canopy vegetation indices over AERONET sites. *Remote Sens. Environ.* **2015**, *162*, 29–44. [[CrossRef](#)]
24. Gorelick, N.; Hancher, M.; Dixon, M.; Ilyushchenko, S.; Thau, D.; Moore, R. Google Earth Engine: Planetary-scale geospatial analysis for everyone. *Remote Sens. Environ.* **2017**, *202*, 18–27. [[CrossRef](#)]
25. Kumar, L.; Mutang, O. Google Earth Engine Applications since Inception: Usage, Trends, and Potential. *Remote Sens.* **2018**, *10*, 1509. [[CrossRef](#)]
26. Nouri, H.; Beecham, S.; Anderson, S.; Nagler, P. High Spatial Resolution WorldView-2 Imagery for Mapping NDVI and Its Relationship to Temporal Urban Landscape Evapotranspiration Factors. *Remote Sens.* **2014**, *6*, 580–602. [[CrossRef](#)]
27. Jensen, J.R. *Introductory Digital Image Processing A Remote Sensing Perspective*, 4th ed.; Pearson: Glenview, IL, USA, 2016.
28. Bunting, P. Atmospheric and Radiometric Correction of Satellite Imagery (ARCSI). Available online: <https://arcsi.remotesensing.info/> (accessed on 10 January 2020).
29. Frantz, D.M.; Stellmes, M.; Hostert, P. A Global MODIS Water Vapor Database for the Operational Atmospheric Correction of Historic and Recent Landsat Imagery. *Remote Sens.* **2019**, *11*, 257. [[CrossRef](#)]

30. Leutner, B. Package ‘RStoolbox’. Available online: <https://cran.r-project.org/web/packages/RStoolbox/RStoolbox.pdf> (accessed on 10 January 2020).
31. De Keukelaere, L.; Sterckx, S.; Adriaensen, S.; Knaeps, E.; Reusen, I.; Giardino, C.; Bresciani, M.; Hunter, P.; Neil, C.; Van der Zande, D.; et al. Atmospheric correction of Landsat-8/OLI and Sentinel-2/MSI data using iCOR algorithm: Validation for coastal and inland waters. *Eur. J. Remote Sens.* **2018**, *5*, 525–542. [CrossRef]
32. Conrad, O.; Bechtel, B.; Bock, M.; Dietrich, H.; Fischer, E.; Gerlitz, L.; Wehberg, J.; Wichmann, V.; Böhner, J. System for Automated Geoscientific Analyses (SAGA) v. 2.1.4. *Geosci. Model Dev.* **2015**, *8*, 1991–2007. [CrossRef]
33. DigitalGlobe Atmospheric Compensation. Available online: http://digitalglobe-marketing.s3.amazonaws.com/files/documents/DataSheet_AComp_DS.pdf (accessed on 7 January 2020).
34. Grizonnet, M.; Michel, J.; Poughon, V.; Inglada, J.; Savinaud, M.; Cresson, R. Orfeo ToolBox: Open source processing of remote sensing images. *Open Geospat. Data Softw. Stand.* **2017**, *2*, 15. [CrossRef]
35. MODIS Land Surface Reflectance. Available online: <http://6s.ltdri.org/> (accessed on 10 January 2020).
36. Orfeo Toolbox. Open Source Processing for Remote Sensing Images. Available online: <https://www.orfeo-toolbox.org/> (accessed on 10 January 2020).
37. TOA Radiance Reflectance Conversion of KOMPSAT 1.5. 2018. Available online: <http://www.si-imaging.com/resources/?pageid=2&uid=284&mod=document> (accessed on 2 May 2019).
38. KOMPSAT-3A Image Data Manual v1.4. 2017. Available online: <http://www.si-imaging.com/resources/?pageid=4&uid=234&mod=document> (accessed on 2 May 2019).
39. OTB Cook Book. Available online: <https://www.orfeo-toolbox.org/CookBook/CompilingOTBFromSource.html#compilingfromsource> (accessed on 30 March 2020).
40. Reference Solar Spectral Irradiance: ASTM G-173. Available online: <https://rredc.nrel.gov/solar/spectra/am1.5/ASTMG173/ASTMG173.html> (accessed on 10 October 2019).
41. NDVI, Mapping a Function over a Collection, Quality Mosaicking. Available online: https://developers.google.com/earth-engine/tutorial_api_06 (accessed on 4 January 2020).
42. USGS Landsat 8 Surface Reflectance Tier 1. Available online: https://developers.google.com/earth-engine/datasets/catalog/LANDSAT_LC08_C01_T1_SR (accessed on 10 January 2020).
43. U.S. Landsat Analysis Ready Data: U.S. Geological Survey Fact Sheet 2018–3053. Available online: <https://pubs.er.usgs.gov/publication/fs20183053> (accessed on 10 January 2020).
44. CEOS Analysis Ready Data. Available online: <http://ceos.org/ard/> (accessed on 30 March 2020).
45. EarthExplorer Homepage. Available online: <https://earthexplorer.usgs.gov/> (accessed on 30 March 2020).
46. 6 Spectral Indexes on Top of NDVI to Make Your Vegetation Analysis Complete. Available online: <https://eos.com/blog/6-spectral-indexes-on-top-of-ndvi-to-make-your-vegetation-analysis-complete/> (accessed on 30 March 2020).



© 2020 by the authors. Licensee MDPI, Basel, Switzerland. This article is an open access article distributed under the terms and conditions of the Creative Commons Attribution (CC BY) license (<http://creativecommons.org/licenses/by/4.0/>).